ELSEVIER

International Journal of Solids and Structures 41 (2004) 4299–4320

INTERNATIONAL JOURNAL OF SOLIDS and STRUCTURES

www.elsevier.com/locate/ijsolstr

Mechanics of Smart-Cut® technology

Xi-Qiao Feng [a,*], Y. Huang [b]

[a] *Key Lab of Failure Mechanics of Education Ministry of China, Department of Engineering Mechanics, Tsinghua University, Beijing 100084, PR China*

[b] *Department of Mechanical and Industrial Engineering, University of Illinois at Urbana-Champaign, Urbana, IL 61801, USA*

Received 20 February 2004; received in revised form 20 February 2004
Available online 17 April 2004

Abstract

Smart-Cut® is a recently established, advanced technology for fabricating high-quality silicon-on-insulator (SOI) systems and has found many other successful applications. It meets almost all the high requirements for processing and manufacturing SOI wafers, which provide the basis of ultra-large-scale integration device structures of modern microelectronic industry. In the present paper, we present a fundamental study on the basic mechanisms in the Smart-Cut technology from the viewpoints of mechanics and physics. First, a model for defect nucleation induced by hydrogen ion implantation is established based on the continuum mechanics theory accounting for the crystal structure of silicon. This model is used to provide an upper bound on the implantation dose of hydrogen ions, one of the most important process parameter in the Smart-Cut technology. An analytical formulation is derived to calculate the defect density as a function of the H-implantation dose and the temperature. Then, the splitting of SOI wafers in the Smart-Cut technology is analyzed using the elastic fracture mechanics theory. Accounting for the embrittlement and diffusion effects of hydrogen, a lower bound of the implantation dose of hydrogen ions is derived, which agrees reasonably with experimental observations. Furthermore, the effects of the handle wafer adopted in the Smart-Cut technique are examined on the splitting process. It is found that the handle wafer leads to uniform crack propagation and higher uniformity in the thickness of the final SOI systems, in comparison with conventional techniques to produce SOI substrates, and prohibits the blistering and flaking failure of an H-implanted wafer. This work provides not only a fundamental understanding to the physical mechanisms associated with the Smart-Cut technology but also a useful reference for determining the process parameters of SOI industrial production.

Keywords: Crack; Debonding; Fracture; Stress intensity factor; Micro-mechanics; Analytic solution; Chemo-mechanical process; Semiconductor material

1. Introduction

Owing to the processing and manufacturing requirements for ultra-large-scale integration (ULSI) device structures, rapid progresses on the silicon-on-insulator (SOI) technology in the semiconductor industry

* Corresponding author. Tel.: +86-10-6277-2934; fax: +86-10-6278-1824.
E-mail address: fengxq@tsinghua.edu.cn (X.-Q. Feng).

0020-7683/$ - see front matter © 2004 Elsevier Ltd. All rights reserved.
doi:10.1016/j.ijsolstr.2004.02.054

have been made during the last two decades. SOI technology has substantial advantages over traditional bulk Si processing for a wide range of ULSI applications (Colinge, 1991; Yankov and Mändl, 2001; Haisma and Spierings, 2002). A typical SOI system consists of a thin layer of single-crystal silicon supported by an underlying insulator (e.g., SiO_2). SOI-based integrated circuits possess such advantages as high speed, high packing density, immunity from latch-up, low power dissipation and high resistance to ionising radiation. Two conventional and commercially available techniques to produce SOI substrates are the separation-by-implanted oxygen (SIMOX) method and the bonded silicon-on-insulator (BSOI) method (Colinge, 1991). The SIMOX process synthesizes an SOI structure with a buried oxide layer by use of very high dose oxygen ion implantation (about 1.0×10^{18} cm^{-2}) and high temperature annealing (1300–1400 °C). The most frequently employed BSOI process, called wafer-bonding-and-etch-back (BESOI), involves chemical removal of a certain part of the device wafer by etching. A serious shortcoming of SIMOX is the very high cost of SIMOX substrates due to its time-consuming and expensive instruments needed, whereas common problems encountered in BSOI are associated with thickness variations of the Si layer and formation of defects (voids, bubbles or microcracks) at the interface between the two starting wafers. Yet none of these conventional fabrication techniques meet all the requirements for ULSI applications.

Recently, a novel and very attractive technique for fabricating high-quality SOI systems has been developed by Bruel, Aspar and their co-workers at LETI (Bruel, 1995, 1996, 1999; Bruel et al., 1997; Aspar et al., 1996, 1997, 1999, 2001). This process, Smart-Cut® as a registered trademark of SOITEC, combines skillfully hydrogen implantation and wafer bonding. It involves basically four main steps, as schematized in Fig. 1 (e.g., Bruel, 1995, 1996, 1999; Bruel et al., 1997; Kozlovskii et al., 2000).

(i) A wafer *A* capped with a dielectric layer (e.g., thermally-grown SiO_2) is exposed to hydrogen implantation at room-temperature with a dose in the range 3.5×10^{16}–1.0×10^{17} cm^{-2} in order to introduce a thin layer with hydrogen ions of sufficiently high density.

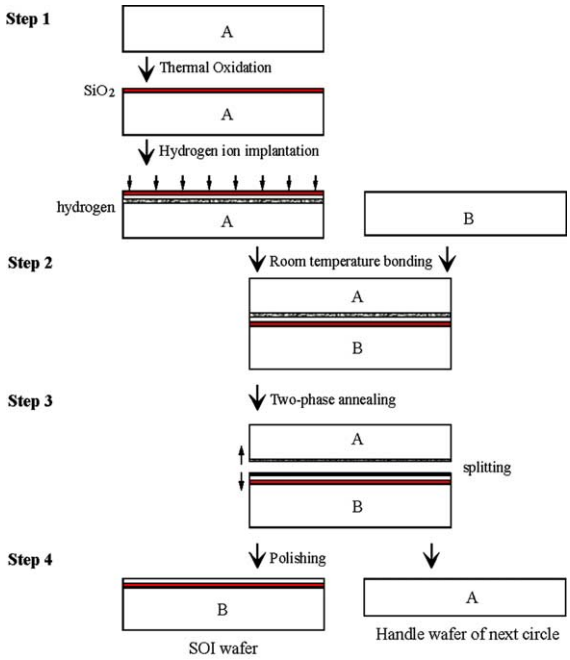

Fig. 1. Schematic of the Smart-Cut process.

(ii) The second step consists of chemical cleaning and hydrophilic bonding at room temperature of wafer A to a handle wafer B by van der Waals forces. The handle wafer serves as a stiffener and provides the bulk silicon beneath the buried SiO_2 in the final SOI structure.
(iii) The third step consists of splitting and annealing of the two bonded wafers including two stages of heating, a medium-temperature stage (400–600 °C) and a high-temperature stage (about 1100 °C). During the first stage, a thin damaged layer appears at the depth of the maximum hydrogen ion concentration in the implanted wafer A, which splits into two parts yielding an SOI structure and the remainder of wafer A. The subsequent high-temperature thermal treatment removes radiation defects in the silicon layer and strengthens the chemical bonds between the two wafers.
(iv) The top silicon layer is polished by a chemical-mechanical method to obtain a high-quality surface. Thus, as a result of the process, an SOI wafer and a residual wafer A are obtained, and the latter can be used again as a handle wafer.

The basic principle of the Smart-Cut technology is suitable for different kinds of applications involving fabrication of single-crystal silicon or semiconductor films transferred onto different types of substrates (e.g., glass and metals) (Bruel, 1995, 1996, 1999; Aspar et al., 1996, 1997, 1999, 2001; Tong and Bower, 1998; Tong et al., 1998, 2000). UNIBOND SOI wafers are produced using the Smart-Cut technology (AubertonHerve et al., 1997; Maleville et al., 1997). This technique has several substantial advantages over the conventional SOI synthesis methods (Bruel, 1996, 1999). First, a high degree of uniformity of the top silicon layer may be achieved by controlling the implantation energy of hydrogen ions. The difference between the maximum and the minimum thicknesses is generally less than 4 nm, in comparison to the relatively large value (20–30 nm) of such conventional methods as SIMOX and BSOI. Second, the SOI systems have high crystalline quality owing to the use of medium implantation doses of light ions and the final fine polishing. Third, ULSI devices made on the Smart-Cut wafers exhibit electrical characteristics comparable to or even better than those of devices made on bulk silicon wafers. Fourth, from the viewpoint of industrial production, all the basic steps involved in Smart-Cut process can be performed on standard microelectronics facility equipment. In comparison of SIMOX, the Smart-Cut technology uses much lower (two orders of magnitude) hydrogen doses and does not need wafer heating during implantation, and, therefore, reduces significantly the cost of fabrication. Fifth, an additional economic advantage of the Smart-Cut process over BESOI technologies is that no wafer is wasted in grinding and thinning operations and one bulk silicon wafer yields one SOI wafer, whereas in BESOI techniques two bulk wafers are needed to get one SOI wafer.

Since its first publication (Bruel, 1995), the Smart-Cut technology has attracted increasingly intensive attentions and has found practical applications in the field of SOI. This technique has already been used in the industrial production of SOI structures since 1997 (Kozlovskii et al., 2000). Using the Smart-Cut technique, Tong and Bower (1998), Tong et al. (2000) transformed Si, Ge, and SiC films on substrates of a high-melting glass. The feasibility of applying the Smart-Cut technique to structured and patterned thin silicon films has also been demonstrated (Aspar et al., 1996, 1999; Yun et al., 1999). Successful application of the Smart-Cut technique for production of SOI structures has stimulated a great interest to develop this method for synthesizing other layered and even three-dimensional structures of semiconductors on insulators. Aspar et al. (1999) and Jalaguier et al. (1998) obtained some new structures with thin films of Si, GaAs or InP on silicon substrates by using the Smart-Cut technique combined with metal bonding. Di Cioccio et al. (1996, 1997, 1998) demonstrated that the Smart-Cut technology can be used for the production of "silicon carbide-on-insulator" structures. By implanting erbium into the top layer of a Smart-Cut SOI wafer, very recently, Gad et al. (2003) fabricated single-mode SOI waveguides with good optical quality.

Even though the Smart-Cut technique has several successful applications as aforementioned, its underlying physical mechanisms have not been well understood yet. The fundamental understanding of the

basic mechanisms of the Smart-Cut technology will be evidently and significantly beneficial for further production process development and large-scale implementation of this novel technique. Up to today, however, studies on this subject are still very limited. Aspar et al. (1997) investigated experimentally the behavior of cavities induced by H-implantation in silicon and examined the effect of a handle wafer on the splitting mechanism. Freund (1997) provided a lower bound estimate on the implantation dose of hydrogen ions, by considering the growth of a circular crack driven by the hydrogen gas induced pressure in the crack. Similar methods have been adopted by Han and Yu (2001) and Yang (2003). Using a combination of spectroscopic and microscopic technique, Weldon et al. (1997, 1998) investigated systematically the thermal evolution of hydrogen implanted into a silicon wafer, as a function of implantation dose, depth, and annealing temperature. They found the chemical action between the implanted hydrogen ions and Si atoms. More recently, Zheng et al. (2001) examined the orientation effect on blistering phenomenon associated with implanted hydrogen in a Si wafer. They found that the blistering has the fastest speed in (1 0 0) Si wafers because of the orientation dependence of the blistering kinetics. Höchbauer et al. (2002a) investigated the physical mechanism behind the ion-cut by studying the cracking depth as a function of H-implantation dose and relating the observed results to damage evolution in the implantation zone and its effects on the (1 0 0) H-platelet formation. Radu et al. (2003) investigated the transfer of GaAs layers onto Si by helium and/or hydrogen implantation and wafer bonding, and obtained the optimum implantation conditions that induce large area exfoliation instead of blistering after annealing of unbonded GaAs.

This work is aimed at providing a systematic mechanics and physics analysis on some basic mechanisms involved in the Smart-Cut process. The outline of this paper is as follows. In Section 2, a model is presented to elucidate the physical mechanisms of defect nucleation induced by hydrogen ion implantation in single-crystal silicon. This model is based on continuum mechanics theory with consideration of crystal structure of silicon. In Section 3, the above model is used to provide an upper bound of hydrogen ion implantation dose needed for splitting a wafer and to estimate the density of defects in an implanted wafer. In Section 4, the splitting of a Smart-Cut wafer is analyzed using the linear elastic fracture mechanics and accounting for the embrittlement and diffusion effects of hydrogen. Then a lower bound on the implantation dose of hydrogen ions is given. In Section 5, the blistering and flaking mechanisms of an implanted wafer are analyzed, and the effects of the handle wafer are examined.

2. Defect nucleation by hydrogen ion implantation

2.1. Effects of hydrogen on defect nucleation

As already mentioned, two key ideas of the Smart-Cut technology are to acquire a large number of microdefects located in a very thin layer in the silicon wafer by H-implantation and thereby to split the wafer system along this layer. Therefore, an insight into the nucleation of microcavities associated with H-implantation is of great interest. Chemical, physical and mechanical considerations are all necessary in order to gain a fundamental understanding of this complicated process occurred at the nanometer scale involving chemical reaction, bond decohesion, and mechanical deformation and fracture. After the hydrogen implantation, the trapped hydrogen atoms or protons combine with silicon atoms to form Si–H complex (Weldon et al., 1997). It should be mentioned that a sufficient energy input is necessary for this process in order to fracture Si–Si bonds and form Si–H bonds. The energy needed is supplied either by thermal energy at a high temperature during the annealing process or by mechanical energy (elastic strain energy) stored in the compound system due to high residual stress (or internal pressure) induced during hydrogen implantation. Microcavity nucleation starts mainly at the late stage of H-implantation and is accelerated by the subsequent thermal treatment. During ion implantation at room temperature, the elastic

strain energy induced by residual stress plays a predominant role in fracture of Si–Si bonds. On the other hand, during high thermal splitting, both thermal and mechanical energy make significant contributions to the fracture process.

Knowledge of the silicon's crystalline structure is useful to the understanding of the defect nucleation process. Silicon possesses a cubic crystal structure of diamond (Cracknell, 1969). A unit cell is schematized in Fig. 2, observed from the $\langle 1\,0\,0\rangle$ direction. The parameters of the unit cell include the lengths $a = b = c = 0.54309$ nm and the angles $\alpha = \beta = \gamma = 90°$. The Si–Si bond length is 0.2352 nm. The unit cell can be divided into eight cube-shaped sub-cells of same size, with the edge length being $a/2$. Each of the four sub-cells with centers located at $(\frac{3}{4}a, \frac{1}{4}b, \frac{1}{4}c)$, $(\frac{1}{4}a, \frac{3}{4}b, \frac{1}{4}c)$, $(\frac{1}{4}a, \frac{1}{4}b, \frac{3}{4}c)$ and $(\frac{3}{4}a, \frac{3}{4}b, \frac{3}{4}c)$ has a body-centered Si atom whereas the other four sub-cells have not. This means that in each unit cell of silicon crystal there are four intrinsic voids (interstitial spacing vacancies) with centers at $(\frac{1}{4}a, \frac{3}{4}b, \frac{3}{4}c)$, $(\frac{3}{4}a, \frac{1}{4}b, \frac{3}{4}c)$, $(\frac{3}{4}a, \frac{3}{4}b, \frac{1}{4}c)$ and $(\frac{1}{4}a, \frac{1}{4}b, \frac{1}{4}c)$, respectively. The void size, to be given below, is comparable to a Si atom but is much larger than a hydrogen ion. Therefore, most hydrogen ions implanted are trapped in these inherent voids, which serve as sources of larger defects.

Hydrogen ions within such an intrinsic vacancy may form hydrogen molecules (Bruel, 1996; Maleville et al., 1997; Varma, 1997). Lusson et al. (1995) performed effusion experiments and Secondary Ion Mass Spectrometry (SIMS) profiling on post-hydrogenated micro-nanocrystallized silicon films obtained by thermal annealing of amorphous sputtered layers. They evidenced the existence of cavities containing molecular hydrogen.

Though no external force is applied on the overall implanted system, the internal pressure of hydrogen gas induces residual stress at the nanometer scale, and therefore provides elastic strain energy for fracture of Si–Si bonds, as discussed earlier. The implantation process pushes more and more hydrogen ions into the voids, causing the increase of internal pressure. The trapped hydrogen atoms diffuse and agglomerate near the peak implantation region during thermal annealing, forming microvoids filled with H_2 molecules (Weldon et al., 1997; Wang et al., 2003). The high pressure inside the microcavities, which is magnified significantly during thermal splitting, is the driving force for nucleation and expansion of defects.

As is well known, single-crystal silicon has a relatively high strength, with a theoretical strength about 7 GPa (Petersen, 1982). However, the implanted hydrogen has an embrittlement effect, which significantly lowers the fracture stress of silicon. The hydrogen ions or molecules may react with silicon to form Si–H bonds following fracture of Si–Si bonds (Weldon et al., 1997, 1998; Henttinen et al., 2002). The embrittlement effect of hydrogen also depends strongly on the temperature. Therefore, there exist two synergistic physical mechanisms by which the implantation of hydrogen may induce nucleation and growth of

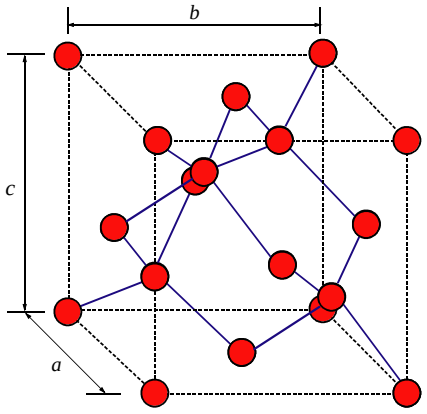

Fig. 2. A cubic unit cell of crystal structure of silicon, viewed from the $\langle 1\,0\,0\rangle$ direction.

nano-sized defects in silicon wafer, namely, the internal pressure of molecule hydrogen in microvoids to provide the driving force for fracture of Si–Si bonds and the hydrogen embrittlement effect to significantly reduce the fracture resistance.

Such a nucleation process occurs at the nanometer scale and involves complex physical and chemical mechanisms. Atomistic studies such as molecular dynamic simulation seem appropriate to investigate the microstructure evolution of a silicon wafer during H-implantation and the subsequent thermal splitting. However, atomistic studies are generally very time-consuming due to the relatively large size and relatively long time involved in the Smart-Cut process. To gain a fundamental and quantitative understanding of defect nucleation and evolution, therefore, we present in the following subsection a continuum mechanics model with microstructure of single-crystal silicon being considered (Jiang et al., in press).

2.2. Model of defect nucleation

Single-crystal silicon wafers currently adopted for SOI devices are generally of high quality and have few defects. Therefore, it is reasonable to assume that all defects are induced merely by hydrogen implantation. We consider an intrinsic void in the silicon crystal filled by hydrogen ions and/or molecules. From the unit cell in Fig. 2, the void radius R_0 can be estimated from the crystal lattice parameter a as

$$R_0 = \frac{\sqrt{3}}{8}a = 0.1176 \text{ nm}, \tag{1}$$

which is comparable to the silicon atom radius (0.110 nm) but much larger (140 times in volume) than the hydrogen atom radius (0.025 nm). The hydrogen-induced internal pressure p in the void is approximately governed by the following equation for a perfect gas:

$$pV = n_{\mathrm{H}_2}\kappa T, \tag{2}$$

where V is the void volume, n_{H_2} the number of hydrogen molecules, T the absolute temperature, and $\kappa = 1.38065 \times 10^{-23}$ J/K the Boltzmann's constant. The ideal gas assumption of molecular hydrogen in microdefects or microcracks has been adopted by Freund (1997), Varma (1997), Yang (2003) and some others.

Owing to its cubic crystal structure, the single-crystal silicon is approximated by a linearly elastic and isotropic solid with Young's modulus E and Poisson's ratio v. At the early stage of defect nucleation, the volume fraction and density of defects are very small such that the effect of defect interaction is negligible and we may consider a spherical void subjected to an internal pressure p in an infinite elastic matrix. The linear elasticity solution gives the nonzero stress and displacement components in a spherical coordinate system (r, θ, φ) as (Timoshenko and Gere, 1961)

$$\sigma_r = -\frac{pR^3}{r^3}, \quad \sigma_\theta = \sigma_\varphi = \frac{pR^3}{2r^3}, \tag{3}$$

$$u_r = \frac{(1+v)pR^3}{2Er^2}, \tag{4}$$

respectively, where R is the void radius after deformation due to the internal pressure, and r the distance from the void center. Note that the void radius R may have a distinct difference from its initial radius R_0 (prior to deformation) due to the high pressure p responsible for the fracture of Si–Si bonds. Therefore, we use the radius R after deformation in Eqs. (3) and (4) to partially account for this geometric effect of void radius. The exact solution based on the finite deformation elasticity theory for a spherical void under internal pressure is given, for completeness, in Appendix A. However, it shows that the formulation in this section has a sufficient accuracy for the current study.

Then the void radius R is obtained from Eq. (4) as

$$R = R_0 + u_r|_{r=R} = R_0\left[1 - \frac{(1+v)p}{2E}\right]^{-1}. \tag{5}$$

The void volume after deformation is given by

$$V = \frac{4\pi}{3}R^3 = \frac{4\pi R_0^3}{3}\left[1 - \frac{(1+v)p}{2E}\right]^{-3}. \tag{6}$$

Its substitution into Eq. (2) gives the governing equation for the internal pressure p

$$\frac{4\pi R_0^3 p}{3}\left[1 - \frac{(1+v)p}{2E}\right]^{-3} = n_{H_2}\kappa T, \tag{7}$$

which has the following solution for p as a function of the number of hydrogen molecules n_{H_2} and temperature T

$$p = \left[\frac{4\pi R_0^3}{3} + \frac{3n_{H_2}\kappa T(1+v)}{2E}\right]^{-1} n_{H_2}\kappa T \tag{8}$$

under the assumption that the internal pressure p is much less than the Young's modulus E. Therefore, the maximum circumferential tensile stress in the material is given by

$$\sigma_{max} = \sigma_\theta|_{r=R} = n_{H_2}\kappa T\left[\frac{8\pi R_0^3}{3} + \frac{3n_{H_2}\kappa T(1+v)}{E}\right]^{-1}. \tag{9}$$

Owing to the brittleness of silicon, we take a maximum tensile stress criterion for defect nucleation

$$\sigma_{max} = \sigma_c, \tag{10}$$

with σ_c being the fracture stress of silicon. σ_c is significantly lower than the theoretical fracture stress due to the hydrogen embrittlement effect. The dependence of σ_c upon the hydrogen ion density and temperature is still an open problem and is beyond the scope of this paper.

Eqs. (9) and (10) give the critical number of hydrogen molecules for defect nucleation (fracture of Si–Si bonds):

$$n_{H_2}^c = \frac{8\pi R_0^3\sigma_c}{3\kappa T}\left[1 - \frac{3(1+v)\sigma_c}{E}\right]^{-1}. \tag{11}$$

We examine the critical number $n_{H_2}^c$ of hydrogen molecules for the following representative parameters: Boltzmann's constant $\kappa = 1.38065 \times 10^{-23}$ J/K, radius $R_0 = 0.1176$ nm, Young's modulus $E = 166$ GPa, Poisson's ratio $v = 0.17$, and fracture stress $\sigma_c = 1.0$ GPa. We consider temperature $T = 298$ K and 773 K, corresponding, respectively, to the room-temperature (25 °C) and thermal annealing (500 °C). Eq. (11) gives $n_{H_2}^c$ as 3.2 at room-temperature and 1.2 at thermal annealing. This suggests that at room temperature (25 °C), a defect will form (e.g., fracture of Si–Si bonds) at the position of an intrinsic vacancy if four or more hydrogen molecules are trapped, while at the annealing temperature (500 °C), two hydrogen molecules located in a vacancy will cause defect nucleation. According to the theory of statistics and probability, the density of vacancies having at least two hydrogen molecules is much higher than that of vacancies having at least four hydrogen molecules. Therefore, heating will significantly accelerate the defect nucleation process by many times, as will be shown below.

It should be pointed out that the critical number of hydrogen molecules, $n_{H_2}^c$, is approximately proportional to the fracture stress σ_c. We have taken a representative value $\sigma_c = 1.0$ GPa, which is around 1/7 of the theoretical strength of Si. Other estimates of σ_c will lead to different predictions of n_c, but they are all around a few (hydrogen molecules). In spite of that the ideal gas approximation and the continuum

mechanics assumption have been adopted, it will shown in the sequel that the results of the present study have a reasonable agreement with experimental observations and numerical solutions.

3. An upper bound estimate of the implantation dose

3.1. Upper bound of the implantation dose

According to the above analysis, the four intrinsic vacancies in each unit cell of single crystal silicon serve as the potential sites of defect nucleation. On one hand, the final splitting of silicon wafer in the Smart-Cut process requires sufficient numbers of defects in the thin layer that has a peak concentration of hydrogen molecules. On the other hand, too many defects in the wafer may lead to undesired defect growth and coalescence, and even the formation of macroscopic defects (e.g., blistering and flaking) prior to annealing. Therefore, the implantation dose is one of the most important process parameters in the Smart-Cut technique, and it should be controlled within an appropriate range. It is of interest to determine theoretically the upper and lower bounds of the implantation dose for hydrogen ions.

We develop a theoretical model for implantation dose of hydrogen in this section. Experimental studies have shown that most hydrogen ions are concentrated in a thin layer (about 100–200 nm thickness) which, depending on the energy of the implanted hydrogen ion beam, is several hundreds nanometers or a few microns below the surface of an implanted wafer (Bedell and Lanford, 2001; Wang et al., 2003). It can easily be shown from energy balance that if the frictional resistance is assumed to be constant during the penetration of a hydrogen ion into single-crystal silicon, the penetration depth of the hydrogen ion, d_H (Fig. 3(a)), is a linear function of the implantation energy without any dependence on the implantation dose. This means that the depth of the peak concentration layer of hydrogen, d_H, is related to the implanted energy U_H by

$$d_H = C_{im} U_H, \tag{12}$$

where C_{im} is a constant associated with friction between penetrating hydrogen ions and single-crystal silicon. Such a linear relation has been verified experimentally (Bruel, 1996; Bedell and Lanford, 2001). From these measurement results, the parameter C_{im} is fitted as about 9–10 nm/KeV, depending upon the

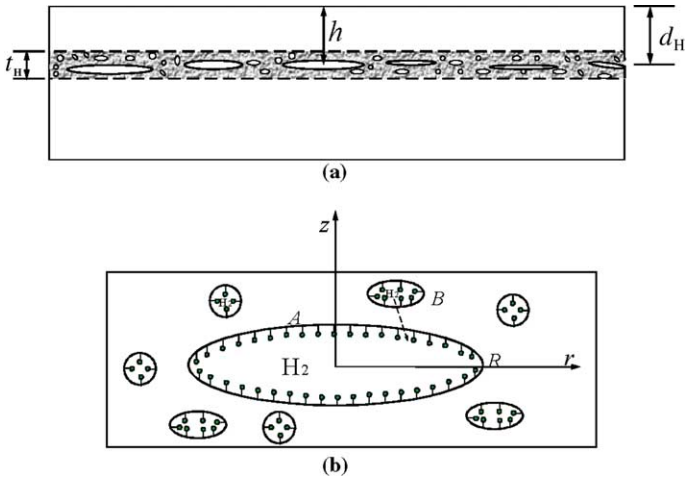

Fig. 3. (a) Microcracks and microvoids distributed in the peak-hydrogen concentration layer and (b) cracks with Si–H bonds on the crack surfaces.

implantation conditions. Taking $U_H = 60$ KeV, for instance, Eq. (12) leads to $d_H = 540$ nm, which agrees well with observations of Wang et al. (2003). Therefore, the implantation energy of hydrogen ions necessary for a desired structure can be easily estimated from the linear relationship in Eq. (12).

Furthermore, the distribution of hydrogen within the peak-concentration layer is homogeneous in the whole sense but highly heterogeneous at the nano-scale. It is just for this reason that hydrogen-induced defects with size of nanometers are distributed randomly within the peak-hydrogen concentration layer. The number density of defects, to be calculated in the sequel, constitutes another important parameter in the Smart-Cut process.

The value of $n^c_{H_2}$ obtained in Eq. (11) may lead to an upper bound of the H-implantation dose, D_H. As a rough approximation, we assume that all the hydrogen ions or atoms are located in a thin layer of thickness t_H (Fig. 3(a)), and that each intrinsic vacancy of crystal structure in this layer has the same number of hydrogen atoms, $n^c_{H_2}$. Therefore, an upper bound of the implantation dose of hydrogen ions is given by

$$D_H^{upp} = 2n^c_{H_2} n_{void} t_H, \tag{13}$$

where n_{void} denotes the number density of intrinsic voids (or vacancies) per unit volume of single-crystal silicon. Since each unit cell has four intrinsic vacancies (as shown in Fig. 2), n_{void} is calculated by

$$n_{void} = 4/a^3 = 2.498 \times 10^{22}\ \text{cm}^{-3}. \tag{14}$$

For representative values $t_H = 100$ nm and $n^c_{H_2} = 1.2$, the upper bound estimate in Eq. (13) gives $D_H^{upp} = 6.0 \times 10^{17}\ \text{cm}^{-2}$, which is larger than the actual necessary dose (3.5×10^{16}–$1.0\times10^{17}\ \text{cm}^{-2}$). This is reasonable because, as aforementioned, it is absolutely unnecessary (and impossible) for all intrinsic spacing vacancies to become defects at the same time. It is sufficient to split the implanted wafer when only a very small fraction (e.g., less than 1%) of intrinsic voids evolve into microdefects because the splitting process is dominated by the growth and coalescence of these defects during thermal annealing, rather than defect nucleation. Nevertheless, Eq. (13) provides a useful reference for estimating the upper bound of hydrogen ion implantation.

3.2. Density of defects

As mentioned before, the implantation dose D_H of hydrogen ions in industrial production is generally in the range between 3.5×10^{16} and $1.0\times10^{17}\ \text{cm}^{-2}$. According to experimental measurement of hydrogen distribution in implanted wafers, most of the hydrogen ions are located in a thin layer about 100–200 nm thickness. The average number of hydrogen ions implanted in each void is

$$n_H = \frac{D_H}{t_H n_{void}}. \tag{15}$$

If we take the representative values $D_H = 1.0 \times 10^{17}\ \text{cm}^{-2}$, $t_H = 100$ nm and $n_{void} = 2.498 \times 10^{22}\ \text{cm}^{-3}$ given in Eq. (14), we find that $n_H = 0.4$, which, as expected, is lower than the upper bound $2n^c_{H_2}$.

Based on the above analysis, we now estimate the density of defects induced by implanted hydrogen ions, d_{defect}, which is defined as the number of intrinsic vacancies per unit area of the water, resulting from fracture of Si–Si bonds (Aspar et al., 1997). We assume that all implanted hydrogen ions are randomly located in all intrinsic voids of the peak-concentration layer. A defect forms at the site of a vacancy once the number of hydrogen ions in it reaches the critical value $2n^c_{H_2}$. Thus, the expected value of the defect density can be obtained either by the theory of probability or Monte-Carlo numerical simulation. Both the methods have been adopted in our study, and their results agree reasonably. However, only the former is presented briefly here because it may lead to a simple analytical solution.

For the problem that hydrogen ions of number $m_{\text{ion}} = D_{\text{H}}/t_{\text{H}}$ are randomly located in voids of number n_{void}, the mathematical expectation value of the number density of voids that contains hydrogen ions no less than $2n^{\text{c}}_{\text{H}_2}$ is expressed as (Haigh, 2002)

$$d_{\text{defect}} = n_{\text{void}} t_{\text{H}} \left[1 - \sum_{\alpha=0}^{2n^{\text{c}}_{\text{H}_2}-1} C^{\alpha}_{m_{\text{ion}}} \left(\frac{1}{n_{\text{void}}} \right)^{\alpha} \left(\frac{n_{\text{void}} - 1}{n_{\text{void}}} \right)^{m_{\text{ion}}-\alpha} \right]. \tag{16}$$

Since both n_{void} and m_{ion} are very large number and $m_{\text{ion}}/n_{\text{void}} < 1$, the number density of defects in Eq. (16) can be calculated more easily by

$$d_{\text{defect}} = n_{\text{void}} t_{\text{H}} \left[1 - \sum_{\alpha=0}^{2n^{\text{c}}_{\text{H}_2}-1} \frac{1}{\alpha!} \left(\frac{m_{\text{ion}}}{n_{\text{void}}} \right)^{\alpha} \exp\left(-\frac{m_{\text{ion}}}{n_{\text{void}}} \right) \right]. \tag{17}$$

Using Eq. (17) and taking the representative values $D_{\text{H}} = 1.0 \times 10^{17}$ cm^{-2} and $t_{\text{H}} = 100$ nm, the defect density is plotted in Fig. 4 with respect to the critical parameter $2n^{\text{c}}_{\text{H}_2}$, which decreases with temperature. For instance, it is estimated from Eq. (17) that the defect density at room temperature after implantation is only 2.88×10^9 cm^{-2} but reaches 1.95×10^{14} cm^{-2} at 500 °C during thermal annealing, that is, the defect nucleation is accelerated by about five orders by heating. The latter number of defect number density indicates that only a very small fraction of intrinsic vacancies (less than 1%) will undergo fracture of Si–Si bonds and become defects, which will expand and coalesce to form microcracks. These two numbers agree reasonably well with the transmission scanning microscopy experimental observations (Aspar et al., 1997; Raineri et al., 2000), though they are slightly larger than the experimental data for several reasons discussed in the following. First, a certain fraction of implanted hydrogen ions are located out of this thin layer, and do not cause defects. Second, if two or more neighboring vacancies form defects, they will coalesce to form a larger defect. Third, it is possible for hydrogen ions diffuse into a defect from its neighboring vacancies (e.g., Lanzavecchia and Colombo, 1996), and therefore the nucleation of a defect may impede nucleation of new defects in a small neighboring region. In addition, if two defects are very near in spacing, hydrogen ions or molecules may diffuse from one defect into another due to their possible difference in internal pressure. Thus one defect will expand while the other will shrink or even disappear. This is referred to as the Ostwald ripening mechanism (Raineri et al., 2000; Grisolia et al., 2000, 2001), which also results in a decrease in the defect number that can be observed.

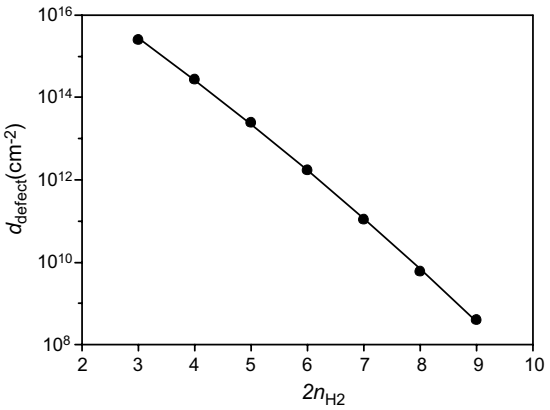

Fig. 4. The defect density in an implanted wafer as a function of the critical number of hydrogen ions.

4. Fracture mechanics analysis of splitting

A high dose of hydrogen or other ion implantation in materials can induce visible macroscopic effects such as blistering, swelling, flaking and exfoliation (Tong et al., 1998; Gösele and Tong, 2000; Bedell and Lanford, 2001). The use of hydrogen ion implantation and the formation of a buried damaged layer along which splitting of a wafer occurs are the key links of the Smart-Cut technology.

The effect of splitting of a wafer along the damaged (or porous) layer is based on the phenomenon of pore coarsening (i.e., growth and coalescence of microvoids), which occurs anisotropically and mainly parallel to the surface of the wafer (Kozlovskii et al., 2000; Wang et al., 2003). Growth and coalescence of microvoids leads to formation of microcracks (Feng and Yu, 2002), which are basically aligned in the same direction, as shown in Fig. 3(a). Wang et al. (2003) observed that most defects in the damaged layer are platelet-like, parallel to the wafer surface, about 0.3–0.6 nm wide and 5–20 nm long. These microcracks are filled with hydrogen molecules (H_2) and are coated with atomic hydrogen captured at broken and dangled Si bonds at the pore surface and at the crack tip (Weldon et al., 1997; Kozlovskii et al., 2000). As already mentioned, hydrogen molecules provide a high internal pressure to drive the crack propagation, while hydrogen atoms bonded with Si at the crack tip decreases greatly the fracture resistance. Analysis of mechanisms associated with such cracks is of considerable interest not only for better understanding the Smart-Cut technology but also for other implantation-based manufacture techniques of SOI (Kozlovskii et al., 2000). Using Griffith's fracture mechanics theory, Freund (1997) performed a theoretical analysis of a crack driven by internal pressure by implanted hydrogen in a wafer. Thereby, he gave a lower bound on the hydrogen dose for splitting a wafer. A similar analysis can be found in Yang (2003). However, the effects of hydrogen embrittlement and diffusion have not been taken into account. In this section, we provide a more comprehensive, though also simple, analysis for possible mechanisms of crack propagation in a damaged layer in a silicon wafer.

In the Smart-Cut process and other ion implantation-based manufacture techniques of SOI, cracks in the damaged layer are desired to grow in a plane parallel to the surfaces of wafers. The (1 0 0) plane of crystal structure of a wafer is usually used as its base plane. Bruel (1995) reported that in the Smart-Cut process, microcrack formation and propagation in H-implanted Si wafers often favor the (1 0 0) plan, with relatively few along the (1 1 1) plane, although the two easiest cleavage planes of single-crystal silicon are (1 1 1) and (1 1 0). Zheng et al. (2001) comparatively examined the H-implantation induced blistering and layer splitting process for (1 0 0), (1 1 1) and (1 1 0) wafers. They showed that the blistering kinetics is clearly orientation dependent, with (1 0 0) Si having the fastest splitting rate, followed by (1 1 1) and (1 1 0) Si. Experimental observations (Aspar et al., 1997; Yun et al., 1999) also confirmed that most microcracks are, as desired, aligned parallel to the wafer surface, i.e., along the (1 0 0) plane, and only a small minority of defects lie on the (1 1 1) plane. This alignment should be attributed to the ability of hydrogen to form Si–H bonds that tend to perpendicular to the (1 0 0) plane.

The fracture strengths of single-crystal silicon are slightly different in (1 0 0), (1 1 1), and (1 1 0) planes. The critical stress intensity factors K_{Ic} of single-crystal silicon are 0.91, 0.94 and 0.83–0.95 MPa $\mathrm{m}^{-1/2}$ along the (1 0 0), (1 1 0) and (1 1 1) planes, respectively (Ericson et al., 1988). Formation of Si–H bonds at the crack tips will decrease the fracture toughness $K_{\mathrm{Ic}}^{(1\,0\,0)}$ most significantly due to their orientation, where the superscript stands for the corresponding plane. Because there are a large number of defects located in the thin damaged layer, their interaction will also make the crack propagation easier in the desired (1 0 0) plane than in other directions.

A hydrogen-driven crack growth can be analyzed according to the linear elastic fracture mechanics. Consider a single circular crack filled by hydrogen molecules and coated with Si–H complex, as shown in Fig. 3(b). The interaction with other cracks is neglected. At the early stage of crack propagation, the crack depth, $h \approx d_{\mathrm{H}}$, is much larger than the crack radius R due to the presence of the handle wafer. The crack can

then be regarded as a mode-I crack embedded in an infinite elastic body. Under the internal pressure p, its mode-I stress intensity factor is (Tada et al., 2000):

$$K_{\mathrm{I}} = 2p\sqrt{\frac{R}{\pi}}, \tag{18}$$

and its crack opening displacement is

$$b(r) = \frac{8(1-\nu^2)p}{\pi E}(R^2 - r^2)^{1/2}. \tag{19}$$

The opening volume of the crack is easily obtained from Eq. (19) as

$$V = \frac{16(1-\nu^2)pR^3}{3E}. \tag{20}$$

Using Eqs. (18) and (20), in conjunction with the ideal gas equation in (2), the stress intensity factor can be re-expressed as

$$K_{\mathrm{I}} = \frac{1}{2R}\sqrt{\frac{3n_{\mathrm{H}_2}E\kappa T}{\pi(1-\nu^2)}}. \tag{21}$$

The fracture criterion of a crack is taken as

$$K_{\mathrm{I}} = \alpha_{\mathrm{H}} K_{\mathrm{Ic}}^{(1\,0\,0)}, \tag{22}$$

where the parameter α_{H} accounts for the embrittlement effect of hydrogen. The circular crack with the radius R will propagate once the number of hydrogen molecules in it reaches a critical value given by

$$n_{\mathrm{H}_2}^{\mathrm{low}} = \frac{4\pi(1-\nu^2)R^2}{3E\kappa T}[\alpha_{\mathrm{H}} K_{\mathrm{Ic}}^{(1\,0\,0)}]^2. \tag{23}$$

When the fracture criterion (22) is met, or equivalently when the number of hydrogen molecules reaches the critical value in Eq. (23), a microcrack will propagate and the internal pressure will decrease due to the increase in the opening volume, that is, the driving force for crack propagation is nonconservative. On the other hand, the decrease of the internal pressure generally means a lower potential energy, therefore providing a driving force for hydrogen diffusion. In order to determine a lower bound of implantation dose, it is of interest to consider the mechanisms of hydrogen diffusion between a main crack and the nearby microcracks, as shown in Fig. 3(b). Basically, hydrogen can be diffused from one crack (say, B) to another (say, A) only when the following conditions are satisfied: (1) a high temperature to provide sufficient activation energy to overcome the resistance to diffusion, (2) a sufficiently large difference of potential or pressure between A and B, and (3) a relatively small spacing between the two cracks. In addition, it is possible for those hydrogen atoms bonded with silicon atoms to evaporate and agglomerate to hydrogen molecules and to diffuse, but this feedback mechanism needs more energy input (Varma, 1997). Experimental observations also found that some hydrogen ions diffuse out of the wafer system (Höchbauer et al., 2001a, 2002b). For these reasons, only a relatively small fraction of hydrogen can be diffused into the main crack from its neighboring regions. We introduce a parameter α_{dif} to signify the ratio of the number $2n_{\mathrm{H}_2}$ of hydrogen atoms that can be diffused into the main crack and the total number of hydrogen atoms implanted in the region beside the crack, that is

$$\alpha_{\mathrm{dif}} = \frac{2n_{\mathrm{H}_2}}{\pi R^2 D_{\mathrm{H}}}. \tag{24}$$

Thus, by Eqs. (23) and (24) and setting $n_{\mathrm{H}_2} = n_{\mathrm{H}_2}^{\mathrm{low}}$, a lower bound of the implantation dose can be obtained as

$$D_{\mathrm{H}}^{\mathrm{low}} = \frac{2n_{\mathrm{H}_2}^{\mathrm{low}}}{\pi R^2 \alpha_{\mathrm{dif}}} = \frac{8(1-\nu^2)}{3\alpha_{\mathrm{dif}} E\kappa T}\left[\alpha_{\mathrm{H}} K_{\mathrm{Ic}}^{(100)}\right]^2, \tag{25}$$

which is inversely proportional to the temperature of thermal splitting and the Young's modulus of silicon.

Under the above approximations of hydrogen diffusion, the stress intensity factor of the crack can be rewritten in terms of the implantation dose as

$$K_{\mathrm{I}} = \left[\frac{3\alpha_{\mathrm{dif}} D_{\mathrm{H}} E\kappa T}{8(1-\nu^2)}\right]^{1/2}, \tag{26}$$

which, surprisingly and interestingly, remains a constant during crack propagation. In fact, under the approximation of α_{dif} being constant, the internal pressure p in the crack can be re-expressed in terms of the implantation dose as

$$p = \left[\frac{3\pi\alpha_{\mathrm{dif}} D_{\mathrm{H}} E\kappa T}{32R(1-\nu^2)}\right]^{1/2}, \tag{27}$$

that is, $p \propto R^{-1/2}$. Therefore, it is evident from Eqs. (18) and (27) that K_{I} is unrelated to the crack radius. The constant value of K_{I} and the zero value of K_{II} ensure crack propagation in a stable manner along the direction parallel to the surface, and therefore lead to a high quality (low roughness of nanometers) of splitting surface and a high uniformity in thickness. This is very crucial for smooth splitting of wafers of large diameters up to 200–300 mm. Since the diffusion rate of hydrogen is a function of temperature and the density of hydrogen atoms, the actual crack growth rate depends on the implantation dose and the annealing temperature.

The fact that the stress intensity factor K_{I} remains a constant during crack growth results from the stiffening effect of the handle wafer. If no handle wafer is introduced, the crack cannot be assumed to be embedded in an infinite body, and the crack will have a mixed-mode crack tip field of mode-I and II, leading to crack kinking and flaking. It is noted that when the crack extends to a length comparable to its distance from the upper surface, the assumption that the crack is embedded in an infinite body becomes inappropriate. The growth of a larger crack will be considered in the next section.

Now we make a quantitative estimation to the lower bound of the implantation dose. For instance, we take the parameter α_{dif} in Eq. (24) to be in the range between 1/4 and 1/2, the hydrogen embrittlement factor in Eq. (23) to be $\alpha_{\mathrm{H}} = 1/4$, and $K_{\mathrm{Ic}}^{(100)} = 0.91\ \mathrm{MPa\,m^{-1/2}}$ (Ericson et al., 1988). The above values of α_{dif} and α_{H} are obtained by fitting various experimental observations on hydrogen effects (Varma, 1997; Höchbauer et al., 2000, 2001a,b, 2002b). Then, the lower bound of the implantation dose of hydrogen ions, $D_{\mathrm{H}}^{\mathrm{low}}$, is in the range of $1.5\text{–}3.0\times10^{16}\ \mathrm{cm^{-2}}$, this compares favorably (as a lower bound estimate) with the actual implantation dose ($3.5\text{–}10.0\times10^{16}\ \mathrm{cm^{-2}}$) in the Smart-Cut process. A lower implantation dose of hydrogen ions indicates that a higher temperature will be needed to achieve the splitting of a silicon wafer.

5. Blistering and flaking of an implanted wafer

5.1. Blistering and planar propagation of a sub-surface crack

Blistering and flaking are two mechanisms often observed during implantation-based manufacture processes (Bruel, 1996; Bedell and Lanford, 2001; Höchbauer et al., 2000, 2002b). Blistering occurs when the depth of the damaged layer is small, as in some SOI techniques. In such a situation, the upper silicon layer (either with or without a SiO_2 layer) above a circular crack can be regarded as a circular plate clamped along its edge and subjected to a uniform pressure p, as shown in Fig. 3(b). When the crack size (e.g., in the early stage of damage evolution) or the internal pressure p is small, the deformation in the transverse

direction (normal to the wafer surface) will be relatively small such that no evident blistering phenomenon can be observed. As the crack propagates, however, the thin plate above the crack will experience a mediate or even large deformation, and so the phenomenon of blistering can be observed distinctly (Fig. 5).

When a sub-surface crack is near to the surface, as shown in Fig. 5(a), it is mixed mode, i.e., having both nonzero mode-I and mode-II stress intensity factors. The mode-II stress intensity factor K_{II} increases with the decrease in the ratio h/R. When $h/R \gg 1$, $K_{\mathrm{II}} \approx 0$ and K_{I} is given by Eq. (18). To examine the basic feature of blistering and flaking induced by H-implantation, we now consider another case of $h/R \ll 1$ by adopting the thin-plate assumption (Jensen, 1991; Hutchinson and Suo, 1992). This simulates the case of H-induced fracture of a wafer without a handle wafer. Referring to a polar coordinate system (r, θ, z), the equilibrium equation of a plate can be expressed in terms of displacement as (e.g., Timoshenko and Woinowsky-Kreiger, 1987).

$$\left(\frac{\partial^2}{\partial r^2}+\frac{1}{r}\frac{\partial}{\partial r}+\frac{1}{r^2}\frac{\partial^2}{\partial \theta^2}\right)\left(\frac{\partial^2 w}{\partial r^2}+\frac{1}{r}\frac{\partial w}{\partial r}+\frac{1}{r^2}\frac{\partial^2 w}{\partial \theta^2}\right)=\frac{p}{S}, \tag{28}$$

where w denotes the displacement of the middle surface of the plate in the normal direction, S is the bending stiffness of the plate defined as

$$S=\frac{Eh^3}{12(1-\nu^2)}. \tag{29}$$

The stress distribution in the plate can be obtained in terms of the displacements w by the standard plate theory (e.g., Timoshenko and Woinowsky-Kreiger, 1987).

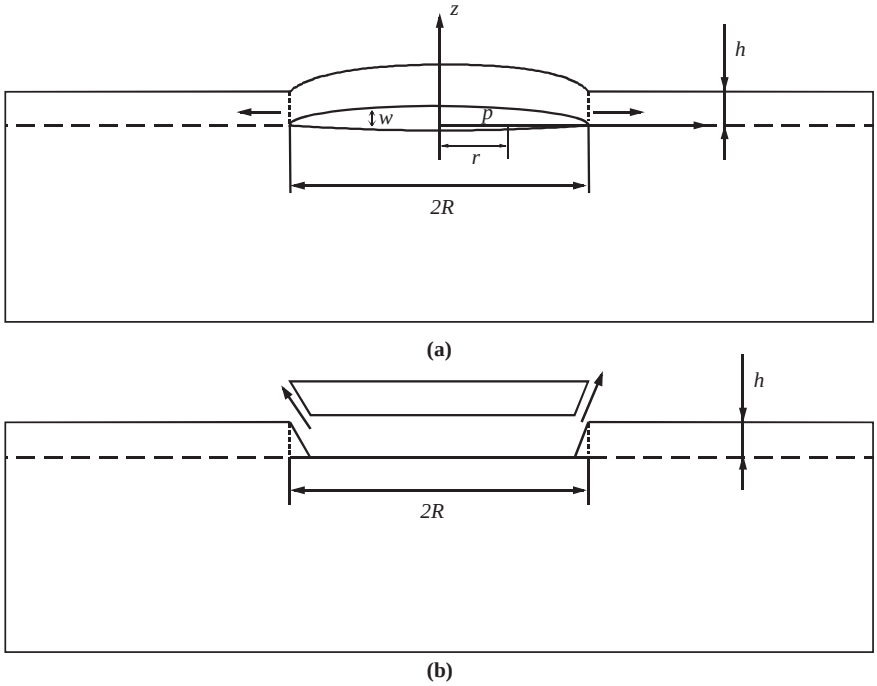

Fig. 5. (a) Planar growth of a sub-surface crack and (b) its flaking.

For the problem of current interest, it is reasonable to assume a clamp-supported boundary condition along the circumference of the plate, that is

$$w|_{r=R} = 0, \ \left.\frac{\partial w}{\partial r}\right|_{r=R} = 0. \tag{30}$$

The middle-surface displacement of the plate subjected to a uniform pressure p can be solved from Eqs. (28) and (30) as

$$w(r) = \frac{p}{64S}(R^2 - r^2)^2. \tag{31}$$

Such a displacement field gives the following bending moment and normal force in the cross section along the clamped boundary ($r = R$) of the circular plate:

$$M_{rr}|_{r=R} = \frac{1}{8}pR^2, \ N_{rr}|_{r=R} = 0. \tag{32}$$

Following the analysis of Jensen (1991) and Hutchinson and Suo (1992), the stress intensity factors of the crack are expressed as

$$\begin{aligned} K_{\mathrm{I}} &= \frac{1}{\sqrt{2}h^{3/2}}(\sqrt{12}M_{rr}\sin\omega - hN_{rr}\cos\omega) = \frac{\sqrt{6}pR^2\sin\omega}{8h^{3/2}}, \\ K_{\mathrm{II}} &= -\frac{1}{\sqrt{2}h^{3/2}}(\sqrt{12}M_{rr}\cos\omega + hN_{rr}\sin\omega) = -\frac{\sqrt{6}pR^2\cos\omega}{8h^{3/2}}, \end{aligned} \tag{33}$$

where the angle $\omega = 52.1^\circ$ for a homogeneous, isotropic and linearly elastic material. The mode mixity of the crack is

$$\tan\psi = \frac{K_{\mathrm{II}}}{K_{\mathrm{I}}} = -\mathrm{cotan}\,\omega, \tag{34}$$

which leads to $\psi = \omega - 90^\circ = -37.9^\circ$.

The displacement in Eq. (31) gives the opening volume of the crack as

$$V = \frac{\pi pR^6}{192S}. \tag{35}$$

Its substitution into Eq. (2) gives the internal pressure:

$$p = \left(\frac{192S}{\pi R^6}n_{\mathrm{H}_2}\kappa T\right)^{1/2}. \tag{36}$$

Using Eqs. (24) and (36), the stress intensity factors in (33) can be rewritten as

$$K_{\mathrm{I}} = \frac{3\sin\omega}{h^{3/2}}\sqrt{\alpha_{\mathrm{dif}}SD_{\mathrm{H}}\kappa T}, \ K_{\mathrm{II}} = -\frac{3\cos\omega}{h^{3/2}}\sqrt{\alpha_{\mathrm{dif}}SD_{\mathrm{H}}\kappa T}. \tag{37}$$

Therefore, the energy release rate of the crack is given by

$$G = \frac{1-v^2}{E}(K_{\mathrm{I}}^2 + K_{II}^2) = \frac{3}{4}\alpha_{\mathrm{dif}}D_{\mathrm{H}}\kappa T. \tag{38}$$

Though the crack is mixed mode, it may still propagate in the (1 0 0) plane which presents as the weakest plane due to the embrittlement effects of hydrogen. Using the following brittle fracture criterion (Hutchinson and Suo, 1992)

$$G = G_c = \frac{1-\nu^2}{E} K_{Ic}^2, \tag{39}$$

the critical implantation dose for crack propagation when $h/R \ll 1$ is determined as

$$D_H^{split} = \frac{4(1-\nu^2)}{3\alpha_{dif} E \kappa T} [\alpha_H K_{Ic}^{(100)}]^2. \tag{40}$$

It is interesting to observe that the critical implantation dose in Eq. (25) for the Smart-Cut process in the presence of a handle wafer is just twice that in Eq. (40) for the crack propagation without the handle wafer. Therefore, due to the stiffening effect of the handle wafer, a higher implantation dose is required for splitting of wafer A in the Smart-Cut process.

5.2. Flaking

Besides planar crack propagation, flaking may occur when the ratio h/R is small, as shown in Fig. 5(b). The maximum tensile stress in the plate above the crack occurs along the circumferential edge, and is expressed as

$$\sigma_{rr}^{max} = \left(\frac{6M_{rr}}{h^2} + \frac{N_{rr}}{h} \right)\Big|_{r=R} = \frac{3p}{4} \left(\frac{R}{h} \right)^2, \tag{41}$$

where Eq. (32) has been used.

Assume that flaking is controlled by the maximum principal stress criterion as

$$\sigma_{rr}^{max} = \sigma_c. \tag{42}$$

Using Eqs. (24), (36) and (41), the critical H-implantation dose for flaking is obtained as

$$D_H^{flake} = \frac{\sigma_c^2 h^4}{54\alpha_{dif} S \kappa T}. \tag{43}$$

The ratio between D_H^{split} for crack propagation (splitting of the wafer) and D_H^{flake} for flaking (failure of the cut process) is

$$\frac{D_H^{split}}{D_H^{flake}} = \frac{6}{h} \left[\frac{\alpha_H K_{Ic}^{(100)}}{\sigma_c} \right]^2. \tag{44}$$

It is observed that for a relatively large thickness h, $D_H^{split} < D_H^{flake}$ such that planar crack propagation plays a dominant role in the splitting process because in this case, the maximum tensile stress occurs in the front of the crack. For a small h, however, blistering and even flaking may occur. This is consistent with experimental observations (Bruel, 1996, 1999; Bruel et al., 1997; Lu et al., 1997).

In summary, if no handle wafer is adopted, H-implantation followed by thermal annealing of a wafer may cause two possible fracture mechanisms, namely, planar crack propagation and flaking. A handle wafer adopted in the Smart-Cut process prohibits the undesired flaking failure and ensures a splitting of high uniformity, yielding an SOI system of good quality. Another effect of the handle wafer is that it decreases the stress intensity factors at the crack tip and, therefore, requires a little higher implantation dose for splitting of the wafer system.

6. Conclusions

Smart-Cut is a novel, advanced production technology of SOI systems. It meets almost all the high requirements for processing and manufacturing SOI wafers, which provide the basis of ULSI device structures. This paper presents a fundamental study on some basic mechanisms in the Smart-Cut technology from the mechanical and physical viewpoints. We have established the following conclusions:

(1) A model for defect nucleation induced by hydrogen ion implantation is established based on the continuum mechanics theory accounting for the effect of crystal structure of Si. An analytical expression is given for estimating the number density of defects. It is found that most defects nucleate in the stage of thermal annealing. For instance, thermal annealing of 500 °C increases the rate of defect nucleation by four or five orders of magnitude. An upper bound on the implantation dose of hydrogen ions is obtained.
(2) The splitting of SOI wafers in the Smart-Cut technology is modeled using the elastic fracture mechanics theory and accounting for the embrittlement and diffusion effects of hydrogen. Though the two easiest cleavage planes of a single-crystal silicon are (1 1 1) and (1 1 0), formation of the Si–H bonds makes the (1 0 0) the desired plane for defect nucleation and crack propagation. Considering the embrittlement and diffusion effects of hydrogen, we have obtained a lower bound of the H-implantation dose, and it agrees well with experimental observations.
(3) The Smart-Cut technique uses a handle wafer as the substrate of the SOI devices. Due to the presence of the handle wafer, cracks in the buried damaged thin layer are mode-I and have a constant value of the stress intensity factor during propagation. This leads to uniform crack propagation in a plane parallel to the wafer surface and high uniformity in the thickness of the final SOI systems. In addition, a handle wafer prohibits the blistering and flaking failure of an H-implanted wafer. This is because, in the absence of handle wafer, a crack under the surface of an H-implanted wafer is mixed mode and the maximum tensile stress along the crack edge is very high to cause flaking. But the handle wafer requires a little higher implantation dose for the splitting of the SOI wafer.

This work provides not only a fundamental understanding to the physical mechanisms associated with the Smart-Cut technique but also a useful reference for determining the process parameters of industrial production, including the implantation dose and energy of hydrogen ions, and the defect density induced by H-implantation and thermal annealing. The temperature of thermal annealing and some other parameters needed for a Smart-Cut process can also be determined by using the model in this paper. Optimization of process parameters is of paramount interest for engineering production of SOI devices to yield low cost and high quality of SOI devices. Further experimental observations and numerical simulation using molecular dynamic or hierarchical calculation methods on the defect nucleation and evolution processes under different process conditions will also be necessary to gain deeper insights in the Smart-Cut technology.

Acknowledgements

X.-Q. Feng acknowledges the support from the National Natural Science Foundation of China (Grant nos. 10121202, 10028204 and 10102008) and the Education Ministry of China (National Excellent Doctoral Dissertation Funding Grant Nr. 199926; Key Grant Project Nr. 0306; and SRFDP Nr. 20030003067). Y. Huang acknowledges the support from NSF (Grant Nr. CMS-0103257) and from NSFC. We also wish to thank Professor H. Gao of Max-Planck Institute of Metals Research at Stuttgart for pointing out some important references on the Smart-Cut Technology.

Appendix A. Finite deformation solution for a spherical void under internal pressure

The exact solution is presented in this Appendix A for a spherical void in an infinite solid subjected to internal pressure p. The solid is isotropic, linearly elastic, but undergoes finite deformation. The reference, undeformed configuration and the current, deformed configuration are shown in Fig. 6(a) and (b), respectively, where R denotes a point in the reference configuration, r the same material point in the current configuration, R_0 and r_0 the radii of the void in the two configurations, respectively. The deformation in the solid is represented by the relation $r = r(R, R_0, r_0)$ to be determined.

Because of spherical symmetry, the true (logarithmic) circumferential strain is related to the stretch r/R in the circumferential direction θ by

$$\varepsilon_\theta = \ln\frac{r}{R}. \tag{A.1}$$

The volume strain is $\varepsilon_r + 2\varepsilon_\theta = \ln\frac{r^2\,\mathrm{d}r}{R^2\,\mathrm{d}R}$, which, in conjunction with (A.1) gives the true strain in the radial direction as

$$\varepsilon_r = \ln\frac{\mathrm{d}r}{\mathrm{d}R}. \tag{A.2}$$

We take a hypoelastic constitutive law which gives the following isotropic, linearly elastic relation between the true (Cauchy) stresses and true (logarithmic) strains:

$$\begin{aligned}\sigma_r &= \frac{E}{(1+v)(1-2v)}[(1-v)\varepsilon_r + 2v\varepsilon_\theta],\\ \sigma_\theta &= \frac{E}{(1+v)(1-2v)}(v\varepsilon_r + \varepsilon_\theta).\end{aligned} \tag{A.3}$$

The equilibrium equation in the current configuration is

$$\frac{\mathrm{d}\sigma_r}{\mathrm{d}r} + \frac{2}{r}(\sigma_r - \sigma_\theta) = 0, \tag{A.4}$$

which can be re-expressed by using Eqs. (A.1)–(A.3) as

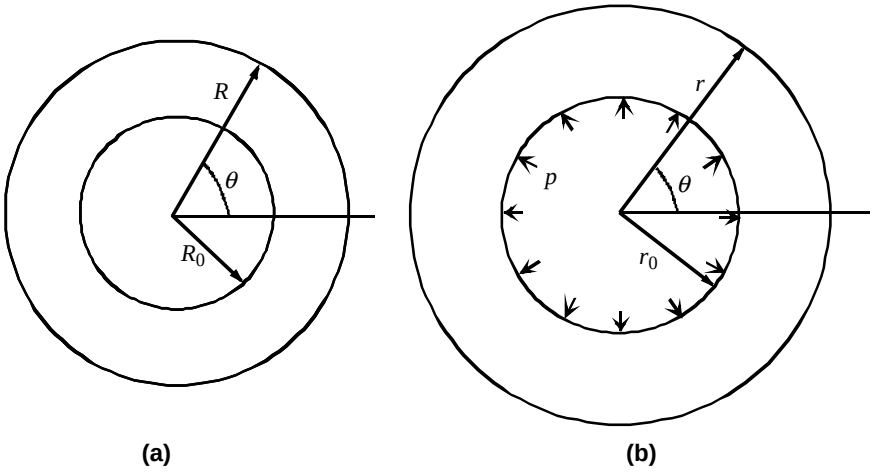

Fig. 6. A spherical void: (a) the reference configuration and (b) the current configuration.

$$\frac{\mathrm{d}}{\mathrm{d}r}\left[(1-v)\ln\frac{\mathrm{d}r}{\mathrm{d}R}+2v\ln\frac{r}{R}\right]+\frac{2}{r}(1-2v)\ln\left(\frac{R}{r}\frac{\mathrm{d}r}{\mathrm{d}R}\right)=0. \tag{A.5}$$

This is the equation governing the relation between the same material point in the current and reference configurations, $r(R)$. In order to solve (A.5) analytically, we introduce the following two variables:

$$X=\ln\frac{r}{r_0},\ Y=\ln\frac{R}{r_0}. \tag{A.6}$$

The governing equation (A.5) for $r(R)$ can now be written in terms of the as-yet-to-be-determined function $Y(X)$ as

$$(1-v)Y''=[(1+v)(1-Y')-2(1-2v)\ln Y']Y', \tag{A.7}$$

where $Y'=\frac{\mathrm{d}Y}{\mathrm{d}X}$ and $Y''=\frac{\mathrm{d}Y'}{\mathrm{d}X}$. The above equation can also be equivalently written as

$$\mathrm{d}Y=\frac{1-v}{(1+v)(1-Y')-2(1-2v)\ln Y'}\,\mathrm{d}Y'. \tag{A.8}$$

Thus, one also has

$$\mathrm{d}X=\frac{1-v}{[(1+v)(1-Y')-2(1-2v)\ln Y']Y'}\,\mathrm{d}Y'. \tag{A.9}$$

The integration of Eqs. (A.8) and (A.9) leads to X and Y expressed in terms of Y' as follows:

$$Y=Y(Y')=\ln\frac{R_0}{r_0}+\int_{Y_0'}^{Y'}\frac{1-v}{(1+v)(1-Y')-2(1-2v)\ln Y'}\,\mathrm{d}Y', \tag{A.10}$$

$$X=X(Y')=\int_{Y_0'}^{Y'}\frac{1-v}{[(1+v)(1-Y')-2(1-2v)\ln Y']Y'}\,\mathrm{d}Y', \tag{A.11}$$

where Y_0' denotes the value of Y' on the void surface. Eqs. (A.10) and (A.11) give the implicit relation between Y and X, $Y(X)$.

The constitutive relation (A.3) can be rewritten in terms of X and Y as

$$\begin{aligned}\sigma_r&=\frac{E}{(1+v)(1-2v)}[(1+v)(X-Y)-(1-v)\ln Y'],\\ \sigma_\theta&=\frac{E}{(1+v)(1-2v)}[(1+v)(X-Y)-v\ln Y'].\end{aligned} \tag{A.12}$$

Then, the stresses and strains can all be expressed in terms of Y' as follows:

$$\begin{aligned}\sigma_r&=\frac{E}{1-2v}\left\{\ln\frac{r_0}{R_0}-\frac{1-v}{1+v}\ln Y'+\int_{Y_0'}^{Y'}\frac{(1-v)(1-Y')}{[(1+v)(1-Y')-2(1-2v)\ln Y']Y'}\,\mathrm{d}Y'\right\},\\ \sigma_\theta&=\frac{E}{1-2v}\left\{\ln\frac{r_0}{R_0}-\frac{2v}{1+v}\ln Y'+\int_{Y_0'}^{Y'}\frac{(1-v)(1-Y')}{[(1+v)(1-Y')-2(1-2v)\ln Y']Y'}\,\mathrm{d}Y'\right\},\end{aligned} \tag{A.13}$$

$$\begin{aligned}\varepsilon_r&=X-Y-\ln Y'=\ln\frac{r_0}{R_0Y'}+\int_{Y_0'}^{Y'}\frac{(1-v)(1-Y')}{[(1+v)(1-Y')-2(1-2v)\ln Y']Y'}\,\mathrm{d}Y',\\ \varepsilon_\theta&=X-Y=\ln\frac{r_0}{R_0}+\int_{Y_0'}^{Y'}\frac{(1-v)(1-Y')}{[(1+v)(1-Y')-2(1-2v)\ln Y']Y'}\,\mathrm{d}Y'.\end{aligned} \tag{A.14}$$

It is also noted that given a value of Y', the coordinates of the corresponding point in the two configurations are determined by

$$R = r_0 \exp\left\{ \int_{Y_0'}^{Y'} \frac{1-v}{(1+v)(1-Y') - 2(1-2v)\ln Y'} \, \mathrm{d}Y' \right\}, \tag{A.15}$$

$$r = r_0 \exp\left\{ \int_{Y_0'}^{Y'} \frac{1-v}{[(1+v)(1-Y') - 2(1-2v)\ln Y']Y'} \, \mathrm{d}Y' \right\}, \tag{A.16}$$

which give implicitly the relation between r and R, $r(R)$.

Finally, we determine the two unknowns Y_0' and r_0 in Eqs. (A.10)–(A.16) from the boundary conditions. The boundary condition on the void surface is $\sigma_r = -p$ at $r = r_0$. This can be written in terms of X and Y as

$$X = 0, \quad Y = \ln\frac{R_0}{r_0}, \quad \sigma_r = -p. \tag{A.17}$$

Similarly, the vanishing of stress in the remote field can be written as

$$X \to \infty, \quad \frac{Y}{X} \to 1, \quad Y' \to 1, \quad \sigma_r \to 0. \tag{A.18}$$

Using the above boundary conditions, in conjunction with Eq. (A.13), the following equations are obtained for determining Y_0' and r_0:

$$\frac{1-v}{1+v}\ln Y_0' - \ln\frac{r_0}{R_0} - \frac{1-2v}{E}p = 0, \tag{A.19}$$

$$\ln\frac{r_0}{R_0} + \int_{Y_0'}^{1} \frac{(1-v)(1-Y')}{[(1+v)(1-Y') - 2(1-2v)\ln Y']Y'} \, \mathrm{d}Y' = 1. \tag{A.20}$$

References

Aspar, B., Bruel, M., Moriceau, H., et al., 1997. Basic mechanisms involved in the Smart-Cut® process. Microelectron. Eng. 36 (1–4), 233–240.

Aspar, B., Bruel, M., Zussy, M., et al., 1996. Transfer of structured and patterned thin silicon films using the Smart-Cut® process. Electron. Lett. 32 (21), 1985–1986.

Aspar, B., Jalaguier, E., Mas, A., et al., 1999. Smart-Cut® process using metallic bonding: application to transfer of Si, GaAs, InP thin films. Electron. Lett. 35 (12), 1024–1025.

Aspar, B., Moriceau, H., Jalaguier, E., et al., 2001. The generic nature of the Smart-Cut® process for thin film transfer. J. Electron. Mater. 30 (7), 834–840.

Auberton–Herve, A.J., Bruel, M., Aspar, B., et al., 1997. Smart-Cut$^{(R)}$: the basic fabrication Unibond® SOI wafers. IEICE T Electron. E 80 (3), 358–363.

Bedell, S.W., Lanford, W.A., 2001. Investigation of surface blistering of hydrogen implanted crystals. J. Appl. Phys. 90 (3), 1138–1146.

Bruel, M., 1995. Silicon-on-insulator material technology. Electron. Lett. 31 (14), 1201–1202.

Bruel, M., 1996. Application of hydrogen ion beams to silicon on insulator material technology. Nucl. Instrum. Methods B 108 (3), 313–319.

Bruel, M., 1999. Separation of silicon wafers by the Smart-Cut method. Mater. Res. Innov. 3 (1), 9–13.

Bruel, M., Aspar, B., Auberton-Herve, A.J., 1997. Smart-Cut: a new silicon on insulator material technology based on hydrogen implantation and wafer bonding. Jpn. J. Appl. Phys. 36 (3B), 1636–1641.

Colinge, J.P., 1991. Silicon-on-Insulator Technology: Materials to VLSI. Kluwer Academic, Boston.

Cracknell, A.P., 1969. Crystals and Their Structures. Pergamon, Oxford.

Di Cioccio, L., Letertre, F., et al., 1996. Silicon carbide on insulator formation using the Smart-Cut process. Electron. Lett. 32 (12), 1144–1145.

Di Cioccio, L., Letertre, F., et al., 1997. Silicon carbide on insulator formation by the Smart-Cut® process. Mater. Sci. Eng. B 46, 349–356.

Di Cioccio, L., Le Tiec, Y., et al., 1998. Silicon carbide on insulator formation by the Smart-Cut® process. Mater. Sci. Forum 264, 765–770.

Ericson, F., Johansson, S., Schweitz, J.-A., 1988. Hardness and fracture toughness of semiconducting materials studied by indentation and erosion techniques. Mater. Sci. Eng. A 105/106, 131–141.

Feng, X.Q., Yu, S.W., 2002. Damage Micromechanics of Quasi-Brittle Solids. Higher Education Press, Beijing.

Freund, L.B., 1997. A lower bound on implant density to induce wafer splitting in forming compliant substrate structures. Appl. Phys. Lett. 70 (26), 3519–3521.

Gad, M.A., Evans-Freeman, J.H., Cinosi, N., et al., 2003. Loss measurements of Er-doped silicon-on-insulator waveguides. Mater. Sci. Eng. B 105, 79–82.

Gösele, U., Tong, Q.Y., 2000. Semiconductor wafer bonding. Annu. Rev. Mater. Sci. 28, 215–241.

Grisolia, J., Ben Assayag, G., Claverie, A., et al., 2000. A transmission electron microscopy quantitative study of the growth kinetics of H platelets in Si. Appl. Phys. Lett. 76 (7), 852–854.

Grisolia, J., Cristiano, F., Ben Assayag, G., et al., 2001. Kinetic aspects of the growth of platelets and voids in H implanted Si. Nucl. Instrum. Meth. B 178, 160–164.

Haigh, J.D., 2002. Probability Models. Springer, London.

Haisma, J., Spierings, G.A.C.M., 2002. Contact bonding, including direct-bonding in a historical and recent context of materials science and technology, physics and chemistry—historical review in a broader scope and comparative outlook. Mater. Sci. Eng. R 37 (1–2), 1–60.

Han, W.H., Yu, J.Z., 2001. Thermodynamic model of hydrogen-induced silicon surface layer cleavage. J. Appl. Phys. 89 (11), 6551–6553.

Henttinen, K., Suni, T., Nurmela, A., et al., 2002. Cold ion-cutting of hydrogen implanted Si. Nucl. Instrum. Meth. B 190 (1–4), 761–766.

Höchbauer, T., Misra, A., Verda, R., et al., 2000. Hydrogen-implantation induced silicon surface layer exfoliation. Philos. Mag. B 80 (11), 1921–1931.

Höchbauer, T., Misra, A., Nastasi, M., et al., 2001a. Investigation of the cut location in hydrogen implantation induced silicon surface layer exfoliation. J. Appl. Phys. 89 (11), 5980–5990.

Höchbauer, T., Misra, A., Verda, R., et al., 2001b. The influence of ion-implantation damage on hydrogen-induced ion-cut. Nucl. Instrum. Meth. B 175, 169–175.

Höchbauer, T., Misra, A., Nastasi, M., et al., 2002a. Physical mechanisms behind the ion-cut in hydrogen implanted silicon. J. Appl. Phys. 92 (5), 2335–2342.

Höchbauer, T., Nastasi, M., Verda, R.D., et al., 2002b. The use of ion channeling and elastic recoil detection in determining the mechanism of cleavage in the ion-cut process. Nucl. Instrum. Meth. B 190 (1–4), 592–597.

Hutchinson, J.W., Suo, Z., 1992. Mixed-mode cracking in layered materials. Adv. Appl. Mech. 29, 63–191.

Jalaguier, E., Aspar, B., Pocas, S., et al., 1998. Transfer of 3 in GaAs film on silicon substrate by proton implantation process. Electron. Lett. 34 (4), 408–409.

Jensen, H.M., 1991. The blister test for interface toughness measurement. Eng. Fract. Mech. 40 (3), 475–486.

Jiang, H., Feng, X.Q., Huang, Y., et al., in press. Defect nucleation in carbon nanotubes under tension and torsion: Stone–Wales transformation. Comput. Meth. Appl. Mech. Eng. 193, in press.

Kozlovskii, V.V., Kozlov, V.A., Lomasov, V.N., 2000. Modification of semiconductors with proton beams. Semiconductors 34 (2), 129–147.

Lanzavecchia, S., Colombo, L., 1996. Hydrogen bonding and migration in amorphous silicon. Europhys. Lett. 36 (4), 295–300.

Lu, X., Cheung, N.W., Strathman, M.D., et al., 1997. Hydrogen induced silicon surface layer cleavage. Appl. Phys. Lett. 71 (13), 1804–1806.

Lusson, L., Elkaim, P., Correia, A., Ballutaud, D., 1995. Hydrogen diffusion and trapping in micro-nanocrystalline silicon. J. Phys. III France 5, 1173–1184.

Maleville, C., Aspar, B., Poumeyrol, T., et al., 1997. Wafer bonding and H-implantation mechanisms involved in the Smart-Cut(R) technology. Mater. Sci. Eng. B-Solid 46, 14–19.

Petersen, K.E., 1982. Silicon as a mechanical material. Proc. IEEE 70 (5), 420–457.

Radu, I., Szafraniak, I., Scholz, R., et al., 2003. GaAs on Si heterostructures obtained by He and/or H implantation and direct wafer bonding. J. Appl. Phys. 94 (12), 7820–7825.

Raineri, V., Saggio, M., Rimini, E., 2000. Voids in silicon by He implantation: from basic to applications. J. Mater. Res. 15 (7), 1449–1477.

Tada, H., Paris, P.C., Irwin, G.C., 2000. The Stress Analysis of Cracks Handbook, third ed. ASME Press, New York.

Timoshenko, S.P., Gere, J.M., 1961. Theory of Elastic Stability. McGraw-Hill, New York.
Timoshenko, S.P., Woinowsky-Kreiger, S., 1987. Theory of Plates and Shells, second ed. McGraw-Hill, New York.
Tong, Q.Y., Bower, R.W, 1998. Beyond Smart-Cut®: recent advances in layer transfer for material integration. MRS Bull. 23 (12), 40–44.
Tong, Q.Y., Huang, L.J., Gösele, U., 2000. Transfer of semiconductor and oxide films by wafer bonding and layer cutting. J. Electron. Mater. 29 (7), 928–932.
Tong, Q.Y., Scholz, R., Gösele, U., et al., 1998. A smarter-cut approach to low temperature silicon layer transfer. Appl. Phys. Lett. 72 (1), 49–51.
Varma, C.M., 1997. Hydrogen-implant induced exfoliation of silicon and other crystals. Appl. Phys. Lett. 71 (24), 3519–3521.
Wang, J., Xiao, Q.H., Tu, H.L., et al., 2003. Microstructure evolution of hydrogen-implanted silicon during the annealing process. Microelectron. Eng. 66 (1–4), 314–319.
Weldon, M.K., Collot, M., Chabal, Y.J., et al., 1998. Mechanism of silicon exfoliation induced by hydrogen/helium co-implantation. Appl. Phys. Lett. 73 (25), 3721–3723.
Weldon, M.K., Marsico, V.E., Chabal, Y.J., et al., 1997. On the mechanism of the hydrogen-induced exfoliation of silicon. J. Vac. Sci. Technol. B 15 (4), 1065–1073.
Yang, F.Q., 2003. Hydrogen-induced silicon wafer splitting. J. Appl. Phys. 94 (3), 1454–1457.
Yankov, R.A., Mändl, S., 2001. Plasma immersion ion implantation for silicon processing. Ann. Phys. Berlin 10 (4), 279–298.
Yun, C.H., Wengrow, A.B., Cheung, N.W., 1999. Ion-cut silicon layer transfer with patterned implantation of hydrogen. Electrochem. Soc. Proc. 3, 125–130.
Zheng, Y., Lau, S.S., Höchbauer, T., et al., 2001. Orientation dependence of blistering in H-implanted Si. J. Appl. Phys. 89 (5), 2972–2978.